Brownian Dynamics Simulations of Dendrimers under Elongational Flow: Bead−Rod Model with Hydrodynamic Interactions

Igor M. Neelov and David B. Adolf*

Department of Physics and Astronomy, University of Leeds, Leeds LS2 9JT, U.K.

Received February 4, 2003; Revised Manuscript Received June 23, 2003

ABSTRACT: Computer simulations of perfectly branched dendrimers up to the sixth generation have been performed under the influence of uniaxial elongational flow for the first time for a model with explicit dendritic topology. The Brownian dynamics simulation technique has been applied to a freely jointed bead−rod model with excluded volume both with and without hydrodynamic interactions. The dependence of conformational properties and the intrinsic elongational viscosity on the flow rate were obtained. The coil−stretch transition was observed for dendrimers of all generations with it being less pronounced than the same type of transition observed for a linear polymer chain. Hydrodynamic interactions shift the onset of this transition to higher elongational rates. The transition is observed to occur in two stages as it was for a linear polymer. The dendrimer first orients at low flow rate as a whole along the flow axis without significant deformation and local orientation. Increasing flow rate leads to local orientation on the level of the monomer leading to significant global deformation of the dendrimer. The monomers belonging to inner generations are oriented stronger relative to outer monomers at all flow rates. The intrinsic elongational viscosity of the dendrimer increases with flow and plateaus at high rates. The limiting value of intrinsic elongational viscosity for a model with hydrodynamic interactions at high flow rates is less than its value for a model without these interactions. The onset of the coil−stretch transition occurs at lower elongational rates as the number of monomers, N, within the dendrimer increases. The dependence of the onset of this transition with N is less pronounced than for a linear chain. It becomes less steep with N and is not described by a power law.

I. Introduction

The behavior of polymers in elongational flow has been of great interest for the past three decades attested to by the numerous experimental, theoretical and computational efforts within this area. It is now well-known that a sharp transition of a flexible macromolecule between a coiled state and a stretched state (i.e., the coil−stretch transition) occurs under the influence of an elongational flow.[1,2] This phenomenon is observed when the elongational rate, $\dot{\epsilon}$, exceeds a critical value, $\dot{\epsilon}_c$, and has been demonstrated for a variety of chemically distinct polymers.[2] Direct visualization of various conformations of a single DNA molecule in an elongational flow are presented in the recent works of Perkins and co-workers.[3,4] A theoretical investigation into the behavior of a linear polymer chain in dilute solution under elongational flow was first performed by de Gennes.[5] Within this effort, the chain is represented as a dumbbell with a conformationally dependent elasticity and friction and the Peterlin−de Gennes approximation (P−dG)[6] is invoked. It was shown that the coil−stretch transition may be continuous ("second order") or discontinuous ("first order"). Similar ideas have been presented by Hinch.[7] A three-dimensional dumbbell model with a conformational dependent friction coefficient was used by Brestkin[8] where the P−dG approximation was not invoked. Magda et al.[9] modified Fixman's technique[10] and applied it to a bead−spring Zimm model with preaveraged hydrodynamic interactions that depended on deformation rate. A sharp steplike transition was obtained for this model. It was revealed that the incorporation of these conformational-dependent hydrodynamic interactions shifted the onset of the coil−stretch transition relative to that predicted by Zimm. Bead−FENE (i.e., finitely extensible nonlinear elastic) spring chains were considered within the theoretical efforts of Wiest et al.[11] It was observed that the coil−stretch transition for this model is gradual and that springs within the middle of the chain were slightly more extended at intermediate flow rates.

Within the last 3 decades, molecular dynamics (MD) and Brownian dynamics (BD) computer simulations methods have been applied to study linear polymer chains in elongational flow. The earlier BD investigations usually did not take into account the hydrodynamic interactions (HI). Acierno et al.[12] and Rallison and Hinch[13,14] simulated bead−rod chains without HI in uniaxial flow and observed that the unfolding of back loops leads to large viscous stresses. Larson developed a simple dynamic kink model[15] to describe this backloop unfolding. Liu[16] proposed an algorithm to simulate the motion of a freely jointed bead−rod chain with constant hydrodynamic interactions in steady-state shear and elongational flow. He observed that for longer chains the coil−stretch transition was sharper and occurred at smaller elongational rates. The rheological and optical behavior of a Kramers bead−rod chain without HI in dilute solution under uniaxial extensional flow were studied by Doyle et al.[17] They showed that the Brownian stress dominates in steady-state uniaxial extensional flow at small flow rates and that the stress−optical law is valid within this region. Larson at al[18] used the BD method to investigate the steady-state extensional behavior of a bead−spring chain model without HI but with a "worm-like" elasticity for each spring. Snapshots of this "worm-like" polymer chain were compared with "snapshots" of a single DNA molecule within elongational flow obtained by Perkins with co-authors within the laboratory. Significant "molecular individualism" [19] was observed arising from a dependence of the onset and the shape of the coil−

10.1021/ma030088b CCC: $25.00
Published on Web 08/09/2003

stretch transition on the initial configuration of the molecule. It was also shown by Neuman[20] that the initial stage of extension of DNA in a steady-state elongational flow is described well by an ideal Gaussian chain. Darinskii and co-workers[21,22] employed Brownian dynamics computer simulations to study a dumbbell with conformational dependent parameters in elongational flow. At elongational flow rates near the critical value, they found that the distribution function of the end-to-end distance is bimodal reflecting the presence of a mixture of coiled and stretched chains.

BD simulations of bead−spring linear polymer chain in elongational flow with rigorous inclusion of HI and excluded volume (EV) have been performed by de la Torre and co-workers[23] over the last 10 years. These studies employed a variety of different soft potentials to constrain the bond lengths (i.e., Rouse, Morse, FENE springs). The transition between coiled and stretched states defined to occur at $\dot{\epsilon}_c$ was obtained as a function of chain length and solvent quality. The steady state and transient rheological behavior of bead−FENE spring chains with and without the inclusion of EV and HI in extensional flow has also been studied by Fetsko and Cummings.[24] The extensibility of the FENE springs was observed to have a pronounced effect on the simulated results by controlling the dependence of the elongational viscosity on elongational rate. Clarification of any confusion generated by this behavior is available only through similar elongational flow simulations using chain models with rigid bond lengths both with and without HI.

To the authors' knowledge, the only simulation of a bead−rod model of a linear polymer chain in elongational flow and in the presence of HI are the two recent efforts of Agarwal et al.[25] and Neelov et al.[26] Agarval et al. used only one chain length of $N = 100$ and EV were not invoked. The SHAKE-HI algorithm[27] was employed which has been criticized from a theoretical viewpoint by Öttinger.[28] The behavior of the chain within the flow was characterized in the first paper solely by the change in the end-to-end distance, which was observed to undergo a sharp coil−stretch transition above a critical elongational rate. Incorporation of HI displaced this value of $\dot{\epsilon}_c$ to higher flow values. Results for intrinsic elongational viscosity were presented only in the absence of HI. In a second paper of Agarval et al.,[25] the behavior of 10 individual chains with different initial conformations was calculated with and without HI. The initial conformation of the chain was observed to influence greatly the chain extension process in agreement with the earlier experimental efforts of Perkins and coworkers and the simulation work of Larson and coworkers.

Neelov et al.[26] used a bead−rod model with HI and EV to study the behavior of chains with lengths ranging from $N = 10$ to nearly $N = 100$ at different elongational flow rates. It was observed that the coil−stretch transition occurs in two stages. At low flow rate, the chain first orients as a whole without significant stretching. With increasing flow rate, orientation increases on the local level leading to substantial stretching of the chain as whole. At intermediate flow rates, the monomer orientation along the chain was observed to be nearly parabolic in shape with a lower extent of orientation located at the chain ends. Substantial increases in the fluctuations in chain size were observed when the flow rate reached its critical value. The dependence of the critical elongational rate on chain length was well described by a power law with exponents of 1.96 and 1.55 for systems performed in the absence and presence of HI, respectively. These values are in good agreement with the previous efforts of de la Torre et al.[23] for a chain consisting of FENE dumbbells in addition to the theoretically predicted values of 2.0 and 1.5 based on Rouse and Zimm models, respectively.

Unlike the situation for linear chain polymers, currently there are no experimental or theoretical efforts dealing with novel polymers like dendrimers and hyperbranched polymers in elongational flow. Novel dendritic structures discovered in 1970s have received particular attention within the past 10 years[29−34] due to their strictly defined structure and size, the existence of internal voids of well-defined size near the core, and the high density of functional terminal groups available. Initially, the primary focus was devoted to the development of different methods of dendritic synthesis. The increased success of these protocols has led to a rapid increase in the number of experimental efforts aimed at identifying applications for these materials. Supramolecular chemistry, drug delivery, and other guest−host applications of dendritic molecules have motivated interest in their equilibrium size, shape, and interior density profiles. Theoretical investigations of dendritic molecules are complicated by the fact that these molecules are typically branched on a scale comparable with or even less than the Kuhn length. This feature underlines the importance of computational studies of these materials. Earlier theoretical studies of de Gennes and Hervet[35] adopted a mean-field model where all the segments belonging to a given generation lie in a concentric shell about a central core. However, efforts of Naylor et al.[36] based on molecular dynamics simulations and molecular mechanics calculations of dendrimers up to generation 7 have revealed open structures rather than a concentric shell assembly. Lescanec and Muthukumar[37] used an off-lattice kinetic growth algorithm to build dendrimers and found a density profile that decreases monotonically outward from the center of the molecule. The dendrimers simulated by Mansfield and Klushin[38] using Monte Carlo (MC) techniques revealed a minimum near the dendrimer center in the density profiles of the higher generation dendrimers studied. These findings were confirmed later by the MC simulations of Lue and Prausnitz.[39] Chen and Cui[40] studied the size of dendrimers as a function of the generation number and length of the spacer between branch points using off lattice MC. Boris and Rubinstein[41] predicted a monotonic decrease in the density profile of a dendrimer using self-consistent mean field techniques. Sheng[42] et al. used off lattice MC with square well potentials to calculate the gyration radius of a dendrimer as a function of the number of monomers, the generation number and the spacer length in good and poor solvents.

Similar issues were addressed by the molecular dynamics simulations of dendrimers in solution performed by Murat and Grest[43] and Mazo et al.[44] Murat and Grest treated the solvent as a continuum. The simulations did not take hydrodynamic interactions (HI) into account and were analyzed primarily in terms of properties such as the radius of gyration and the radial distribution function of monomers.

The dependences of dendrimer size and zero-shear viscosity on number of generations were studied by Mansfield and Klushin[45] using the variational approach of Fixman[46] and in addition to other efforts by Aerts,[47] Widman and Davies,[48] and Cai and Chen.[49] It was observed that intrinsic viscosity as a function of molecular weight (or generation g) in some cases passes through a maximum near $g = 4-5$ in contrast to the behavior of a linear polymer where the intrinsic viscosity is a steadily increasing function of molecular weight. La Ferla[50] extended the Rouse−Zimm dynamical model with preaveraged HI to dendrimers and calculated the viscoelastic relaxation spectrum. Lyulin et al.[51] used Brownian dynamics with fluctuating hydrodynamic interactions to study dendrimers in the absence and presence of a shear flow. It was observed that for a dendrimer in the absence of flow the density of monomers was virtually constant within the interior of the dendrimer due to significant backfolding of the terminal groups. The intrinsic viscosity within the shear flow as a function of g revealed a peak between values of 4 and 5. Lyulin et al.[52] also revealed that the intrinsic viscosity for hyperbranched polymers exhibits a less pronounced peak or plateau at the same generation values where a peak is observed for the corresponding dendrimer. Sheridan et al.[53] used BD with HI to develop empirical relationships that expressed the radii of gyration of trifunctional hyperbranched polymers in terms of the number of monomers, N, within the molecule and the molecule's Wiener index, W. A similar relationship was developed for the hyperbranched polymer's intrinsic viscosity. This effort revealed the dependence of a hyperbranched polymer's intrinsic viscosity vs the number of monomers within the hyperbranched molecule can be linear or peaked depending on the Wiener index of the molecule employed at each generation.

Recently, Lee and McHugh[54] suggested a simplified coarse-grained model of a dendrimer and employed it in BD simulations in the presence of a shear and a uniaxial elongational flow. In this model, all monomers belonging to the same generation of a given dendrimer are replaced by one larger monomer. In effect, the dendrimers are being represented as stars with arms composed of increasingly larger (N.B. from the center to the periphery) beads. HI were accounted in this model through the Oseen−Burgers tensor. Most of the results presented were for a dendrimer within a shear flow but some limited amount of data were published for a dendrimer within an elongational flow. It was obtained that the extensional viscosity for dendrimers of generation numbers 0 through 6 increased with flow. However, the magnitude of this increase was very small in comparison with linear chains.

In this paper, a dendrimer with explicit dendritic topology in elongational flow is simulated for the first time. BD simulation techniques are applied to a freely jointed bead−rod model in the presence of HI and EV. It complements the authors' earlier investigations of dendrimers and hyperbranched polymers[51−53] employing a bead−rod model with EV and HI within a shear flow. In section II, the model of the dendrimer is introduced and the details of the simulation algorithm are explained. The simulated behavior of the dendrimer under elongational flow is reported in section III. A coil−stretch transition was observed for dendrimers of all generations but these transitions occur at higher elongational rates and are less pronounced relative to what is observed for linear chains in elongational flows. The elongational flow rate associated with the onset of the transition (i.e., the critical elongational rate, $\dot{\epsilon}_c$) for the dendrimers decreases with the number of monomers within the dendrimer. However, this decrease is not as steep as observed for their linear cousins and cannot be represented by a power law. A general summary is presented in section IV.

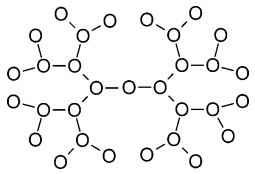

Figure 1. Model of the simulated dendrimer with branching at every bead.

II. Model and Algorithm Details

Brownian dynamics simulations of dendrimers in the presence of elongational flow with branching at every bead have been performed. Figure 1 illustrates a second-generation dendrimer where it is seen that the core is bifunctional, with all other monomers being trifunctional. Monomers are represented by beads with a friction coefficient ζ. Beads are connected by rigid rods of length l and the total number of generations for a given dendrimer is denoted by g. The core is denoted as generation 0 and consists of the central bead and its two immediately bonded neighbors. Torsional and valence angle potentials are not employed. At each integration step, a two-stage procedure was used to generate the new coordinates. First, the unconstrained displacement was calculated using the Ermak-McCamon equation of motion[27]

$$\vec{r}_i = \vec{r}_i^{\,0} + \Delta t/kT \sum_j \mathbf{D}_{ij}^0 \cdot \vec{F}_j^0 + \vec{v}_i^0 \cdot \Delta t + \vec{\Phi}_i^0(\Delta t), \quad i = 0, ..., N \quad (1)$$

where $\vec{r}_i^0$ is the position vector for bead i before the Brownian dynamics time step, Δt, is taken. The core bead is labeled as $i = 0$. k is Boltzmann's constant and T is the simulation temperature. $\mathbf{D}_{ij}^0$ is the diffusion tensor, $\vec{\Phi}_j^0$ is the force on bead i arising from bead j and $\vec{v}_i^0$ is the velocity of the solvent at the position of bead i. For the steady elongational flow studied here

$$v_{i,x}^0 = x_i^0\dot{\epsilon}, \quad v_{i,y}^0 = -0.5y_i^0\dot{\epsilon}, \quad v_{i,z}^0 = -0.5z_i^0\dot{\epsilon}$$

The solvent is represented as a structureless continuum with dendrimer-solvent collisions mimicked by the vector $\vec{\Phi}_i^0$ which has a zero mean and a variance-covariance matrix given by

$$\langle \vec{\Phi}_i^0(\Delta t)\vec{\Phi}_j^0(\Delta t)\rangle = 2\Delta t\mathbf{D}_{ij}^0 \quad (2)$$

where in the absence of HI

$$D_{ii}^{(\alpha\beta)0} = (kT/\zeta)\delta_\alpha\beta, \quad i = 0, ..., N \quad (3a)$$

$$D_{ij}^{(\alpha\beta)0} = 0, \quad i \neq j = 0, ..., N \quad (3b)$$

and $\delta_{\alpha\beta}$ is the Kronecker δ. The constraint forces are computed within the second stage of an integration step in a fashion suggested by Öttinger[28] with a relative tolerance of 2×10^{-6}. A Lennard-Jones potential, U_{LJ},

is invoked

$$U_{LJ} = \sum_{ij} 4\epsilon\left(\left(\frac{\sigma}{r_{ij}}\right)^{12} - \left(\frac{\sigma}{r_{ij}}\right)^{6}\right) \quad (4)$$

between all nonbonded beads i and j with a cutoff distance, r_{cutoff}, of 2.5σ. The parameters $\sigma = 0.8l$ and $\epsilon = 0.3kT$ were used following Rey et al.[55] and the authors' previous work with linear chains in elongational flow.[26] HI are represented rigorously by means of the Rotne−Prager−Yamakawa interaction tensor.[56] The elements of the diffusion tensor are given by eq 5, parts a and b. For the case of nonoverlapping beads (i.e., when $R_{ij} = |\vec{R}_{ij}| = |\vec{r}_i - \vec{r}_j| \geq 2a$) one has

$$D_{ij}^{\alpha\beta} = h^*(\pi/3)^{1/2}(3kT/4\zeta)(l/R_{ij})\left[\left(\delta_{\alpha\beta} + \frac{R_{ij}^{\alpha}R_{ij}^{\beta}}{R_{ij}^{2}}\right) + \frac{2a^2}{3R_{ij}^{2}}\left(\delta_{\alpha\beta} - \frac{3R_{ij}^{\alpha}R_{ij}^{\beta}}{R_{ij}^{2}}\right)\right] \quad (5a)$$

where R_{ij} is the separation between beads i and j each with Stokes' hydrodynamic radius a. α and β represent the x, y, or z components of the vector $\vec{R}_{ij}$. The strength of the HI is set by the parameter $h^* = (3/\pi)^{1/2}a/L = (3/\pi)^{1/2}\zeta/(6\pi\eta_s l)$ where η_s represents the solvent viscosity. A value of $h^* = 0.25$ is employed due to its success within earlier studies using a bead−spring model[23] and a bead rod model.[26,51] This h^* value corresponds to a hydrodynamic radius, a, of $0.257l$. Because of the use of soft intermolecular potentials the beads can overlap (i.e., $R_{ij} < 2a$). In this case[56]

$$D_{ij}^{\alpha\beta} = (kT/\zeta)\left[\left(1 - \frac{9R_{ij}}{32a}\right)\delta_{\alpha\beta} + \left(\frac{3}{32a}\right)\frac{R_{ij}^{\alpha}R_{ij}^{\beta}}{R_{ij}}\right] \quad (5b)$$

In this paper, reduced quantities are reported. All lengths are scaled in terms of the rigid bond length, energy in terms of kT units and friction in terms of the monomer friction coefficient (i.e. $\zeta = 6\pi\pi\eta_s a$ for a monomer where η_s represents the solvent viscosity). It follows that time is scaled by $\zeta l^2/kT$ and elongational flow rate by $kT/\zeta l^2$. Elongational rates spanning a range from 0.0001 to 300 and a time step between $\Delta t = 3 \times 10^{-4}$ and 5×10^{-5} are used within this investigation. The total number of generations within the dendrimers considered in this study ranges from 2 through 6.

A procedure proposed by Murat and Grest is used to generate the initial configurations of dendrimers up to $g = 6$. An equilibration period of 2.5×10^6 to 2.5×10^7 time steps, depending on the dendrimer generation and the elongational rate, was performed before trajectories were saved for analysis. The achievement of steady-state conditions was monitored through the radius of gyration, R_g, the components of the inertia tensor, **T,** and the average distance from the core of the dendrimer to the groups located on its periphery. Following equilibration, production runs were performed and the resulting trajectories analyzed. Each production run was between 5×10^6 and 5×10^7 time steps in length depending on the generation, the elongational rate, and the magnitude of the time step.

The remaining sections of this paper investigate the dependence on elongational rate of the steady-state size, the steady-state shape, and the intrinsic elongational viscosity of the dendrimer. Error bars for all plotted data points are smaller than the size of the symbol used unless otherwise indicated. Furthermore, lines connecting data points within figures are an aid to the eye unless otherwise indicated.

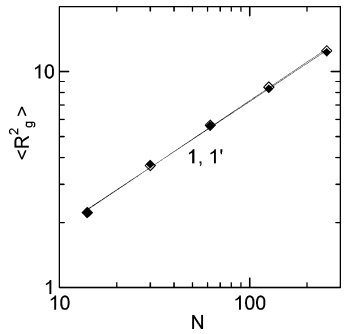

Figure 2. Dependence of the mean squared radius of gyration, $\langle R_g^2\rangle$, of a dendrimer, (diamonds; 1 with HI and 1′ without HI). Filled symbols represent simulations performed with HI whereas open symbols denote simulations performed without HI. The two overlapping solid lines are best fits in each case. The overlapping of the open and closed symbols indicate that the N dependence of $\langle R_g^2\rangle$ is not dependent on the presence or absence of HI.

III. Results and Discussion

1. Characteristics of Dendrimers not under Elongational Flow. Various characteristics of dendrimers of different generations in the absence of flow are first reviewed to validate the model and the simulation method. The variation with the number of monomers, N, of the mean squared radius of gyration, $\langle R_g^2\rangle$, of the dendrimer and the mean squared distance, $\langle R^2\rangle$, between the dendrimer's core and the terminal beads averaged over all terminal beads are shown in Figure 2. Solid best-fit lines of the N dependence of $\langle R_g^2\rangle$ are illustrated for simulations performed in the presence (labeled 1) and absence (labeled 1′) of hydrodynamic interactions. Curves 1 and 1′ overlap each other in Figure 2, revealing that the N dependence of $\langle R_g^2\rangle$ is not dependent on the presence or absence of HI. The data are observed to be consistent with a power law with a best-fit exponent (i.e., slope on the log−log scale) of 0.59 which is in close agreement with the BD result of Lyulin et al. of 0.62 for the same model but with a trifunctional core. These results are also consistent with the MC results of approximately 0.6 due to Mansfield and Klushin and values covering the range of 0.60−0.66 due to Sheng et al. MD simulations due to Murat and Grest of dendrimers with a trifunctional core revealed values of this exponent to be between 0.59 and 0.61. A value of 0.44 has been reported based on a kinetic growth model,[37] and 0.35 in the MC simulation of Chen and Cui in the limit of large N. Theoretical predictions for this exponent are 0.40 from a self-consistent model[35] and 0.356 from an ϵ-expansion[57] all performed in the limit of $N \rightarrow \infty$. Further discussion concerning the values of this power law exponent are found within the work of Sheng et al.[42]

More detailed insight into the dendrimer's internal structure can be obtained from radial distribution functions generated from all monomers and from just the terminal groups. These plots are seen within Figure 3, parts a and b, respectively for dendrimers of generations 2−6. The plots are normalized to have an overall area equal to the number of monomers in the corre-

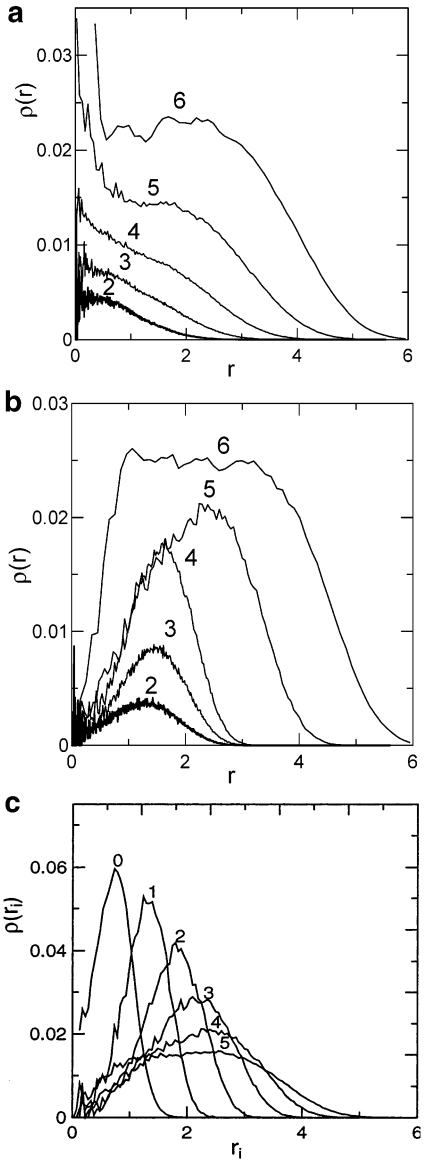

Figure 3. (a) Radial distribution function of bead positions relative to the center of mass for the $g = 2-6$ dendrimers (lines 2−6 respectively) for simulations performed with HI. (b) Distribution function of terminal beads relative to the center of mass for the $g = 2-6$ dendrimers (lines 2−6 respectively) for simulations performed with HI. (c) Distribution function of beads belonging to different generations i ($i = 0, 5$) of a $g = 5$ dendrimer simulated within the presence of HI.

sponding dendrimer, and r is a distance from the dendrimer's center of mass. Good qualitative agreement is observed between these plots and similar plots in the previous BD efforts of Lyulin et al. and the MD efforts of Murat and Grest for dendrimers with a trifunctional core. Figure 3a reveals no dip for dendrimers of generation $g = 2$ through $g = 5$ and a noticeable dip in the density of monomers near the core of the generation $g = 6$ dendrimer. Figure 3b reveals the distribution of terminal groups actually peaks and plateaus throughout the interior of the dendrimer. Figure 3c depicts the distribution of monomers of a fifth-generation dendrimer resolved over each separate generation ($i = 0, ..., 5$). The monomer distribution functions for each separate generation have a symmetric shape with the location of each distribution's peak and the width of each distribution varying significantly. Monomers belonging to generations nearer the core have more peaked

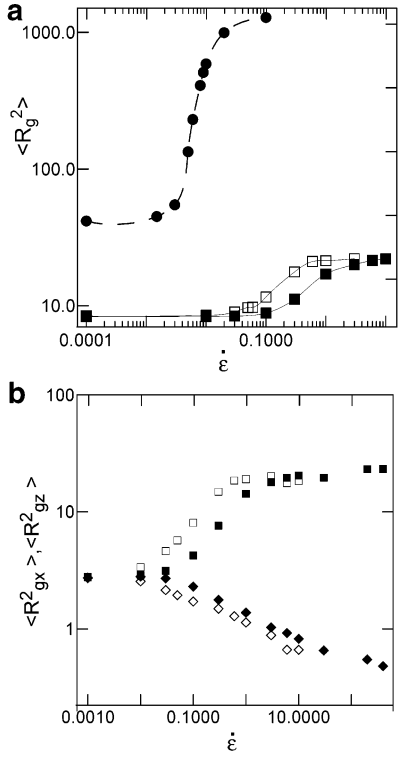

Figure 4. (a) Elongational flow rate dependence of $\langle R_g^2 \rangle$ for a $g = 5$ dendrimer (squares) and for a linear chain (circles) with the same number of monomers (i.e., $N = 127$). Filled symbols represent simulations performed with HI where open symbols denote simulations performed without HI. (b) Elongational flow rate dependence of R_g^2 along the flow direction, $\langle R_{gx}^2 \rangle$ (squares), and perpendicular to the flow direction, $\langle R_{gz}^2 \rangle$ (diamonds), of a $g = 5$ dendrimer. Filled symbols represent simulations performed with HI whereas open symbols denote simulations performed without HI.

distributions and hence are more spatially localized relative to monomers further from the core where distributions functions are observed to overlap more.

2. Characteristics of Dendrimers under Elongational Flow. A. Elongational Rate Dependence of Dendrimer Size. $\langle R_g^2 \rangle$ is plotted in Figure 4a as a function of the elongational rate for a fifth-generation dendrimer with and without HI and for a linear chain simulated in the presence of HI with the same number of monomers (i.e., $N = 127$) with HI. Values close to the unperturbed value of 8.3 are observed for situations with and without HI at small elongational rates (i.e., $\dot{\epsilon} < 0.01$). Increasing the elongational rate leads to a coil−stretch transition and to nearly a 3-fold increase in the radius of gyration at high $\dot{\epsilon}$. However, this increase is significantly smaller and less sharp than for a linear chain in elongational flow. The transition region for a dendrimer spans nearly two decades of $\dot{\epsilon}$ (i.e., $\dot{\epsilon} = 0.1$ to 10) in comparison with approximately 1 decade for a linear chain of the same molecular weight.

These observations are consistent with the fact that the mean squared radius of gyration of a freely jointed linear polymer chain consisting of N monomers in an unperturbed coiled state and in a completely extended state are proportional to N and N^2 respectively. This indicates that their ratio and hence the sharpness of the transition increases as N. The slower increase of this value for dendrimers is partly due to its smaller gyration radius in its completely extended state in comparison with the linear chain with the same number of monomers. But even this value is unattainable due

to the congestion and hence the associated excluded volume interactions preventing total alignment.

Previous efforts with linear chains under elongational flow including those due to the authors of this manuscript[26] revealed HI tended to shift the onset of the coil−stretch transition to higher elongational rates. This shift observed for linear polymer chains is due to the difference between the longest Rouse and Zimm relaxation times as discussed within ref 58. Figure 4a reveals that similar behavior is observed for dendrimers. Analogous plots based on $\langle R^2 \rangle$ rather than $\langle R_g^2 \rangle$ revealed similar behavior and are therefore not shown.

B. Elongational Rate Dependence of Dendrimer Shape. The average shape of the dendrimer as a whole within uniaxial elongational flow can be further characterized quantitatively by components of the mean squared radius of gyration in the direction of the flow, $\langle R_{gx}^2 \rangle$, and that perpendicular to the direction of flow. As the y and z projections are practically indistinguishable, only $\langle R_{gz}^2 \rangle$ is presented as the projection perpendicular to the direction of flow. Values of $\langle R_{gx}^2 \rangle$ and $\langle R_{gz}^2 \rangle$ for a fifth-generation dendrimer are shown in Figure 4b both in the absence of HI (open symbols) and in the presence of HI (filled symbols). Similar plots based on analogous components of $\langle R^2 \rangle$ illustrated similar behavior as will be discussed in the following paragraph and are therefore not shown.

The overall behavior of $\langle R_{gx}^2 \rangle$ and $\langle R_{gz}^2 \rangle$ as a function of elongational rate is qualitatively similar for cases where HI are invoked and where they are neglected. At small elongational rates ($\dot{\epsilon} < 0.001$ for the situation without HI and $\dot{\epsilon} < 0.01$ for the situation with HI), $\langle R_{gx}^2 \rangle = \langle R_{gz}^2 \rangle = \langle R_g^2 \rangle/3$ and equal to their unperturbed values of 2.77. $\langle R_{gx}^2 \rangle$ is observed to increase with increasing elongational rates and plateaus at high elongational rates where the extent of dendrimer deformation is at its highest. The behavior of $\langle R_{gx}^2 \rangle$ is similar to that of $\langle R_g^2 \rangle$ within Figure 4a. However, the magnitude of the transition is larger for $\langle R_{gx}^2 \rangle$ since its plateau value at high elongational flow rate is close to that of $\langle R_g^2 \rangle$ while its value at low elongational flow is one-third the value of $\langle R_g^2 \rangle$. The values of $\langle R_{gz}^2 \rangle$ decrease and approach values nearly 10 times less than values at low flow rates. This decrease of $\langle R_{gz}^2 \rangle$ for the dendrimers is not as dramatic as that observed for linear chains. For linear chains, $\langle R_{gz}^2 \rangle$ is observed to decrease from a scaled unperturbed value equal to the number of monomers N within the chain to values near zero over the same window of elongational rates. However, this decrease of $\langle R_{gz}^2 \rangle$ for the dendrimers is steeper than for the coarser grained dendrimers of Lee and McHugh.[54] HI again only shift the onset of the increase (decrease) in $\langle R_{gx}^2 \rangle$ ($\langle R_{gz}^2 \rangle$) to higher $\dot{\epsilon}$ values as seen to a greater extent in Figure 4a for $\langle R_g^2 \rangle$. Comparing Figure 4a and Figure 4b reveals the onset of the transition occurs at lower $\dot{\epsilon}$ for $\langle R_{gx}^2 \rangle$ than for $\langle R_g^2 \rangle$.

C. Global and Local Orientation of the Dendrimer. The average orientation of the dendrimer as a whole relative to the direction of elongational flow can be characterized by $\langle R_x^2 \rangle / \langle R^2 \rangle$ which can also be written as $\langle \cos^2 \theta_{\mathbf{R}x} \rangle$ where $\theta_{\mathbf{R}x}$ is the angle between the core-to-terminal bead vector and the direction of flow. $\langle \cos^2 \theta_{\mathbf{R}x} \rangle$ for a fifth-generation dendrimer is plotted within Figure 5a (diamonds) for simulations performed in the presence and absence of HI. Both curves illustrate similar features**.** The value of $\langle \cos^2 \theta_{\mathbf{R}x} \rangle$ hovers around its unperturbed value of $^1/_3$ from $\dot{\epsilon} = 0$ to $\dot{\epsilon} < 0.001$ in the absence of HI and up to $\dot{\epsilon} < 0.01$ in the presence of HI. As $\dot{\epsilon}$ increases, $\langle \cos^2 \theta_{\mathbf{R}x} \rangle$ increases and eventually plateaus with HI tending to delay the onset of the transition. This behavior is comparable to that observed for a linear polymer chain (not shown in Figure 5a) but occurs at higher elongational rates than for a linear chain with the same number of monomers. Furthermore, this behavior is qualitatively similar to that observed within Figure 4a for $\langle R_g^2 \rangle$ though for a given dendrimer the onset of the transition occurs at lower elongational flow rates for $\langle \cos^2 \theta_{\mathbf{R}x} \rangle$ than for $\langle R_g^2 \rangle$.

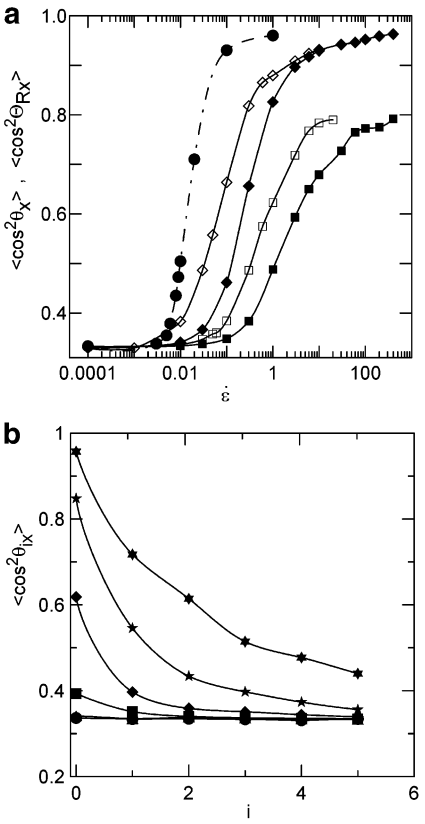

Figure 5. (a) Elongational flow rate dependence of $\langle \cos^2 \theta_{\mathbf{R}x} \rangle$ (diamonds) and $\langle \cos^2 \theta_x \rangle$ (squares) for a $g = 5$ dendrimer. Circles represent $\langle \cos^2 \theta_x \rangle$ for a linear chain simulated in the presence of HI with the same number of monomers as the $g = 5$ dendrimer (i.e., $N = 127$). Filled symbols represent simulations performed with HI whereas open symbols denote simulations performed without HI. (b) $\langle \cos^2 \theta_{ix} \rangle$ as a function of generation number i ($i = 0$, ..., 5) of a fifth-generation dendrimer with HI at elongational flow rates of $\dot{\epsilon} = 0$ (circles), 0.001 (triangles), 0.03 (squares), 0.05 (diamonds), 0.1 (five-pointed stars), and 0.3 (six-pointed stars) listed bottom to top as the lines joining the data appear within the figure.

A similar analysis can be performed using a local orientational angle, θ_x, representing the average angle between unit vectors along the individual rigid bonds of the dendrimer and the flow direction. The quantity $\langle \cos^2 \theta_x \rangle$ for simulations with and without HI is plotted within Figure 5a (squares) for a fifth-generation dendrimer (squares) and for linear chain (circles) of the same number of monomers ($N = 127$) as in dendrimer. This quantity is computed as the ratio $\langle l_x^2 \rangle / \langle l^2 \rangle$ where $\langle l_x^2 \rangle$ is the mean squared x projection of a unit vector along a given bond with brackets denoting an average over all bonds. $\langle l^2 \rangle$ is unity within the current set of dimensionless units.

The general shape of the curves representing the average orientation of the dendrimer as a whole and local orientation of the dendrimer are similar. However,

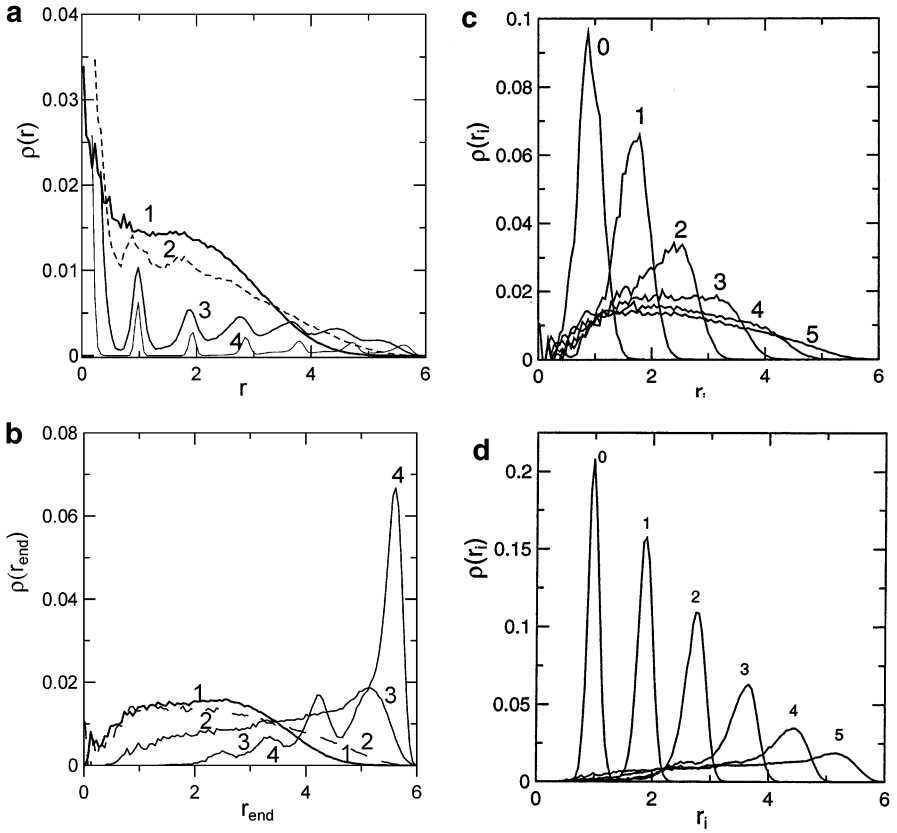

Figure 6. (a) Radial distribution function of bead positions relative to the center of mass for the $g = 5$ dendrimer at the following elongational flow rates: (1) $\dot{\epsilon} = 0.0$, (2) 0.3, (3) 1.0, and (4) 6.0 from simulations performed in the presence of HI. (b) Radial distribution function of terminal bead positions relative to the center of mass for the $g = 5$ dendrimer at the following elongational flow rates: (1) $\dot{\epsilon} = 0.0$, (2) 0.3, (3) 1.0, and (4) 6.0 from simulations performed in the presence of HI. (c) Radial distribution function of beads belonging to different generations ($i = 0-5$) in a $g = 5$ dendrimer from simulations performed in the presence of HI with $\dot{\epsilon} = 0.3$. (d) Same as in part c but at $\dot{\epsilon} = 1.0$.

the transition from randomly oriented bonds (i.e., $\langle\cos^2\theta_x\rangle = {}^1/_3$) to completely oriented bonds $\langle\cos^2\theta_x\rangle = 1$) occurs at a significantly larger $\dot{\epsilon}$ value than the onset of a similar transition in $\langle\cos^2\theta_{\mathbf{R}x}\rangle$. This implies different values of $\dot{\epsilon}_c$ would be predicted depending on whether the onset of the "coil"−stretch transition was detected by the change in $\langle\cos^2\theta_x\rangle$ (e.g., via birefringence data), or by $\langle\cos^2\theta_{\mathbf{R}x}\rangle$. Additionally, the location of an $\dot{\epsilon}_c$ based on $\langle\cos^2\theta_x\rangle$ is numerically close to the onset of the transition in the mean squared radius of gyration, $\langle R_g^2\rangle$, data shown in Figure 4a. Once again HI cause the onset of the transition to be delayed to higher elongational flow rate values.

These observations are qualitatively similar to the authors' earlier findings for a linear chain ($N = 10-94$) within an elongational flow with two significant differences. First, the orientation of monomers within a dendrimer occurs at significantly higher elongational rates relative to linear chains of the same number of monomers. Second, the full local orientation of the monomers within a dendrimer (i.e., squares within Figure 5a) along the flow axis is not achieved due to excluded volume interactions even for significantly deformed dendrimers at high elongational flow rates.

Figure 5b illustrates $\langle\cos^2\theta_{ix}\rangle$ as a function of generation number, i ($i = 0, ..., 5$), for a $g = 5$ dendrimer with HI at different values of the elongational flow. At very low shear rates, values of ${}^1/_3$ are observed reflecting isotropic orientation of the bond vectors with respect to the flow axis within each separate generation. Within increasing flow, the bonds closer to the core (i.e., 1 and 2) orient more than bonds within generations further from the core (i.e., 4 and 5). In particular, it is interesting to note the significantly lower amounts of bond vector orientation within the outermost generations even at elongational flow rates near the middle of the coil−stretch transition.

D. Radial Distribution Function of Internal and Terminal Monomers. Figure 6a illustrates the density distribution function, $\rho(r)$, of monomers as a function of a distance, r, from the fifth-generation dendrimer's center of mass for a variety of elongational rates. The distributions at small elongational rates (line 1) are qualitatively similar to that in the absence of flow (Figure 3a). At elongational rates which correspond to the coil−stretch transition region, this distribution becomes broader with peaks beginning to appear at various positions along the curve (lines 2−4). At the highest rates, the distribution is comprised of a series of separate sharper peaked curves which correspond to the average bead positions in different generations of a dendrimer near complete elongation.

The density distribution function, $\rho(r_{end})$, of terminal groups as a function of a distance r_{end} from the fifth-generation dendrimer's center of inertia is plotted in Figure 6b at the same flow rates as in Figure 6a. At low elongational rates (lines 1 and 2), the plots have a broad plateau at low r_{end} values which is followed by a long tail which decreases to zero at high values of r_{end}. This behavior is similar to that without flow. In contrast, at intermediate flow values (line 3), $\rho(r_{end})$ is observed to slightly increase with increasing r_{end} until

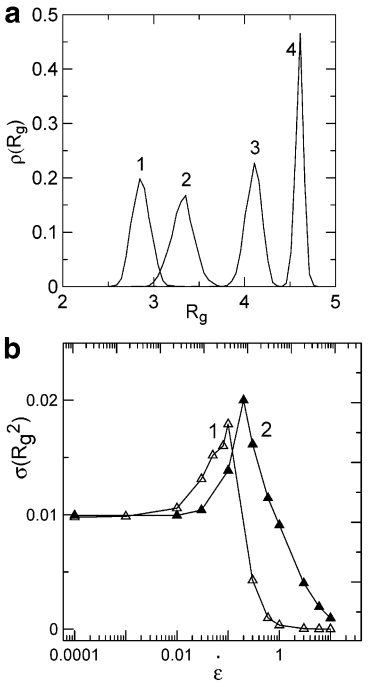

Figure 7. (a) Distribution function of the radius of gyration of a $g = 5$ dendrimer at the following elongational flow rates: (1) $\dot{\epsilon} = 0.0$, (2) 0.3, (3) 1.0, and (4) 6.0 from simulations performed in the presence of HI. (b) Elongational flow rate dependence of the fluctuations of the gyration radius for a $g = 5$ dendrimer. Filled symbols represent simulations performed with HI whereas open symbols denote simulations performed without HI.

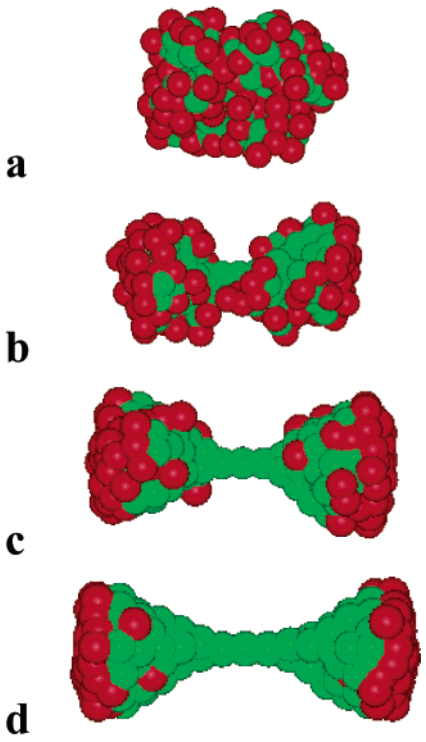

Figure 8. Snapshots of a $g = 6$ dendrimer from simulations performed in the presence of HI at the elongational flow rates of (a) $\dot{\epsilon} = 0.1$, (b) $\dot{\epsilon} = 1$, (c) $\dot{\epsilon} = 6$, and (d) $\dot{\epsilon} = 60$. Red beads within all of these pictures represent monomers within the outermost generation (i.e., terminal units).

it abruptly drops to zero between r_{end} values of 5−6. At high flow rates (line 4), the density of terminal units near the center diminishes forcing more of them to be located at higher r_{end} values. As a consequence, excluded volume interactions within the resulting dense collections of terminal units allows peaks to develop at high r_{end} values with some evidence of backfolding still observed. Further insight into this issue is available if the distribution of monomers, $\rho(r_i)$ ($i = 0, ..., 5$), is plotted for each generation of a fifth-generation dendrimer at different flow rates. At a flow rate of $\dot{\epsilon} = 0.3$ as depicted in Figure 6c, $\rho(r_i)$ is qualitatively similar in appearance to that shown in Figure 3c in the absence of flow. Generations nearer the core reveal more peaked curves in contrast to curves for higher generation numbers where monomers are observed to reside throughout the dendrimer. This picture changes when moving to a high flow rate of $\dot{\epsilon} = 1.0$ as shown in Figure 6d. Relative to Figure 6c, the mixing of monomers from different generations is significantly reduced with the peak intensity at higher generation numbers increasing.

E. Distribution Function and Fluctuations of Gyration Radius. Figure 7a reveals the distribution function of the values of the radius of gyration $\rho(R_g)$ for a fifth-generation dendrimer at different elongational rates, $\dot{\epsilon}$, labeled 1 (lowest) through 4 (highest) on the figure. At elongational flow rates corresponding to the coil−stretch transition (i.e., line 2), $\rho(R_g)$ shifts to high R_g values and broadens slightly. The increased width reflects an increase in the fluctuations of the dendrimer's size in the vicinity of the transition. Further increases in flow rates continues to shift $\rho(R_g)$ to higher R_g values and a narrowing of the width. Figure 7b directly demonstrates the fluctuations of the gyration radius (i.e., $\sigma(R_g^2) = [(\langle R_g^4 \rangle - \langle R_g^2 \rangle^2]^{0.5}$). It can be seen that these fluctuations at flow rates less than roughly 0.001 are the same and independent of flow rate and regardless of whether HI are invoked or not. As the transition region is approached, the fluctuations in $\sigma(R_g^2)$ are observed to increase by a factor of nearly 2 relative to pretransition values. After the peak, $\sigma(R_g^2)$ quickly drops to values near zero. HI are observed to increase slightly the peak magnitude, to shift the position of the peak to higher $\dot{\epsilon}$ values and to slow the drop after the peak.

F. Snapshots of the Dendrimer. Snapshots of a sixth-generation dendrimer with HI at different elongational rates are presented in Figure 8, parts a−d. Figure 8a shows the conformation of dendrimer at an elongational rate of $\dot{\epsilon} = 0.1$ at the onset of the coil−stretch transition. At a higher flow rate of $\dot{\epsilon} = 1.0$ which is near the middle of the coil−stretch transition, Figure 8b reveals the dendrimer is a dumbbell where two "collections" of monomers are joined by a short thick bridge of monomers. This bridge become more and more narrow as the flow rate increases further as seen within Figure 8, parts c and d. Figure 8c corresponds to $\dot{\epsilon} = 6$, which is close to the end of the transition, and Figure 8d to $\dot{\epsilon} = 60$, which is within the completely extended state. The final high flow rate structure can be described as two coaxial cones connected at their tips. Red beads within all of these pictures represent monomers within the outermost generation (i.e., terminal units). The difference in the distribution of terminal units at low and high $\dot{\epsilon}$ values is striking. At $\dot{\epsilon}$ values of 0.1 and 1.0, terminal units are dispersed throughout the dendrimer. At $\dot{\epsilon} = 6$ and 60, most terminal units are found at the outer edge of the coaxial cones. These observations give further insight into the flow-induced formation of peaks within the density distribution functions depicted in Figure 6, parts a and b.

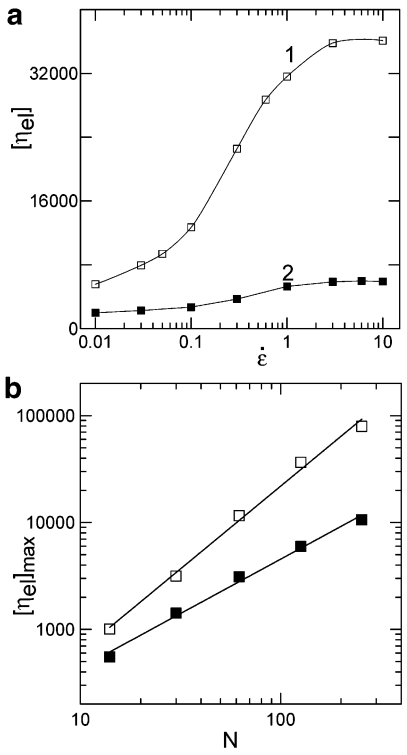

Figure 9. (a) Elongational flow rate dependence of the intrinsic elongational viscosity for a $g = 5$ dendrimer. Filled symbols (curve 2) represent simulations performed with HI whereas open symbols (curve 1) denote simulations performed without HI. (b) Dependence of the plateau values of the intrinsic elongational viscosity, $[\eta_{el}]_{max}$, on the total number of beads within the dendrimer, N. Filled symbols represent simulations performed with HI whereas open symbols denote simulations performed without HI. Best-fit curves are represented by solid lines with slopes of 1.0 and 1.55 for cases with and without HI.

G. Elongational Viscosity. The primary rheological property of interest in this study is the stress tensor, given by the Kramers expression[58]

$$\tau = -\eta_0 \dot{\epsilon} - n\langle \mathbf{RF} \rangle + n\mathbf{I} \tag{6}$$

where $\dot{\epsilon}$ is the rate-of-strain tensor and η_0 is the elongational viscosity of the solvent. For simple elongational flow, $\dot{\epsilon}_{xx} = -2\dot{\epsilon}_{yy} = -2\dot{\epsilon}_{zz} = \dot{\epsilon}$ and all off diagonal components of the rate-of-strain tensor are zero. Here the n is the number density of dendrimer, **RF** is the virial tensor for a single dendrimer. The elongational viscosity is expressed in terms of the elongational stress as

$$\eta_{el} = -\frac{\tau_{xx} - \tau_{zz}}{\dot{\epsilon}} = \eta_0 + n\frac{\langle \mathbf{R}_x\mathbf{F}_x - \mathbf{R}_z\mathbf{F}_z \rangle}{\dot{\epsilon}} \tag{7a}$$

and the corresponding intrinsic elongational viscosity is calculated as

$$[\eta_{el}] = \left[\frac{(\eta_{el} - \eta_0)}{n\eta_0}\right] \tag{7b}$$

The intrinsic elongational viscosity $[\eta_{el}]$ afforded by simulations with and without HI is plotted in Figure 9a for a fifth-generation dendrimer as a function of elongational rate. Each set of data reveals a transition from an unperturbed "coil" at low elongational rates to a highly stretched conformation at high elongational rates. At low elongational flow rates, the viscosity is expected to be constant whereas at higher flow rates it is expected to become flow dependent. Hydrodynamic interactions are observed to displace the occurrence of this transition to higher elongational rates as in earlier figures depicting dendrimer extension and orientation. At very high elongational rates, the plateau value of $[\eta_{el}]$ for the model with HI is observed in Figure 9a to be significantly lower than $[\eta_{el}]$ values without HI. This observation is expected since HI between dendrimer beads acts to decrease dendrimer friction and hence viscosity relative to the case where HI are absent.[58]

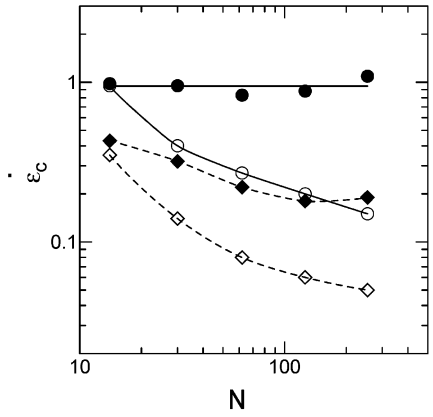

Figure 10. Dependence of the critical value of the elongational flow rate, $\dot{\epsilon}_c$, on the total number of beads within the dendrimer, N. $\dot{\epsilon}_c$ values were defined either at the middle of the transition for $\langle R_g^2 \rangle$ denoted as circles or the onset of the transition in $\langle R_g^2 \rangle$ denoted as diamonds. Filled symbols represent simulations performed with HI whereas open symbols denote simulations performed without HI.

The plateau values of the intrinsic elongational viscosity, $[\eta_{el}]_{max}$, at large elongational rates for dendrimers comprised of $N = 14$, 30, 62, 126, and 254 monomers (i.e., generation $g = 2$, 3, 4, 5, and 6 respectively) are plotted in Figure 9b vs N on a log−log scale. Filled symbols correspond to simulations where HI are invoked with open symbols representing simulations performed in the absence of HI. The lines running through the symbols indicate $[\eta_{el}]_{max} \sim N^{1.55}$ for simulations performed in the absence of HI and $[\eta_{el}]_{max} \sim N^{1.0}$ for simulations performed in the presence of HI. This is in contrast to authors' previous BD simulations of linear chains where $[\eta_{el}]_{max} \sim N^3$ for simulations performed in the absence of HI and $[\eta_{el}]_{max} \sim N^{2.67}$ for simulations performed in the presence of HI. Results for linear chains are in good accordance with theoretical predictions for linear polymers of Larson et al.[59] ($[\eta_{el}]_{max} \sim N^3$) and Bird et al.[58] To the authors' knowledge, there are no theoretical predictions of the limiting viscosity at high elongational rates for dendrimers.

H. Dependences of Critical Transition Rate on Dendrimer Size. Plots of $\langle R_g^2 \rangle$ vs $\dot{\epsilon}$ for the family of dendrimers ranging from the second to sixth generation with and without HI have been constructed. Figure 4a is one such example of these plots. Identifying the critical value of elongational rate, $\dot{\epsilon}_c$, from each of these plots allows the dependence of $\dot{\epsilon}_c$ on generation number to be determined for simulations performed with and without HI. $\dot{\epsilon}_c$ values were defined either at (a) the middle of the transition for $\langle R_g^2 \rangle$ denoted as circles within Figure 10 or (b) the onset of the transition in $\langle R_g^2 \rangle$ denoted as diamonds within Figure 10. Due to the difficulty in locating the onset of the transition to

sufficient accuracy, option b actually defines $\dot{\epsilon}_c$ as the flow rate where $\langle R_g^2 \rangle$ increases to 20% of its pretransition value.

In Figure 10, the critical values, $\dot{\epsilon}_c$,defined using definitions a and b are plotted vs the number of monomers, N, for simulations performed without and with HI. Results for definition a or b reveals that $\dot{\epsilon}_c$ decreases with N for a dendrimer without HI where the steepest descent is observed at low N values. When considering similar data for simulations performed in the presence of HI, $\dot{\epsilon}_c$ data are higher at a fixed value of N relative to simulations performed in the absence of HI. Furthermore, the HI $\dot{\epsilon}_c$ curves are observed to decay more slowly or even remain more or less constant with increasing N relative to runs that did not invoke HI. The lack of linearity in the decays of both sets of $\dot{\epsilon}_c$ data within the log−log plots in Figure 10 reveals that they are not well described by power laws. Comparison to previous work with linear chains[26] reveals the decrease of $\dot{\epsilon}_c$ with N is steeper for linear chains either relative to that observed for the dendrimers in Figure 10 independent of how $\dot{\epsilon}_c$ is determined (see above) and independent of whether HI are present or absent. Furthermore, the decay observed in similar $\dot{\epsilon}_c$ vs N plots for the linear polymer chains illustrated a clear power law behavior with slopes of 1.5 for simulations with HI and 2.0 for simulations without HI in agreement with the theoretical predicition of the Rouse and Zimm models, respectively.

IV. Summary

Brownian dynamics simulations of the statistical and rheological properties of a bead−rod model of a dendrimers of $g = 2-6$ generations with EV under elongational flow have been performed. Both dendrimers with and without HI were studied and compared at different elongational rates. Both the average dendrimer extension and orientation have been calculated as a function of $\dot{\epsilon}$. It is observed that critical values of the elongational rates obtained from dendrimer extension and from the local orientation of the monomers during the "coil"−stretch transition are nearly the same. At the same time, the orientation of the dendrimer as a whole occurs at smaller values of $\dot{\epsilon}$. Inclusion of HI leads to a shift of the "coil"−stretch transition for all these characteristics to higher values of $\dot{\epsilon}$. It was also shown that the bonds belonging to the inner generations of the dendrimer are significantly more oriented in elongational flow relative to bonds belonging to outer generations.

The distribution of the monomer density around the center of mass of the dendrimer develops structure as $\dot{\epsilon}$ is increased. This structure represents monomers within different generations of the dendrimer and becomes increasingly pronounced with further increases in $\dot{\epsilon}$. The peak in the mean squared fluctuations of the gyration radius in the transition region is shifted by HI to higher flow rates. The limiting intrinsic elongational viscosity at high $\dot{\epsilon}$ is significantly smaller for a dendrimer with HI relative to a dendrimer without HI with the N dependence of both being well described by a power law relationship. Finally, the dependence of the critical elongational rate, $\dot{\epsilon}_c$, on N was calculated for the first time for a dendrimer in elongational flow. Findings reveal that dendrimers do not exhibit as steep of a decrease of $\dot{\epsilon}_c$ with N in relation to their linear cousins and that this decay for dendrimers cannot be represented by a power law.

Acknowledgment. The authors acknowledge the EPSRC for financial support of this study (GR/M64215). This work is partly supported by INTAS 00-00712 and the ESF program SUPERNET. I.M.N. is grateful to CSC (Espoo, Finland) for computer time on the parallel IBM SC computer.

References and Notes

(1) Frank, F. C.; Keller, A.; Mackley, M. R. *Polymer* **1971**, *12*, 467.
(2) *Flexible Polymer Chain Dynamics in Elongational Flow: Theory and Experiment*; Nguyen, T. D., Kausch, H. H., Eds.; Springer-Verlag: Heidelberg, Germany, 1999.
(3) Perkins, T. T.; Smith, D. E.; Chu, S. *Science* **1997**, *276*, 2016.
(4) Smith, D. E.; Chu, S. *Science* **1988**, *281*, 1335.
(5) de Gennes, P. G. *J. Chem. Phys.* **1974**, *60*, 5030.
(6) Peterlin, A. *J. Polym. Sci., Polym. Lett.* **1966**, *4*, 287.
(7) Hinch, E. J. *Polym. Lubr., Colloq. Int. CNRS* **1974**, *233*, 241.
(8) Brestkin, Yu. V. *Acta Polym.* **1987**, *38*, 470.
(9) Magda, J. J.; Larson, R. G.; Mackay, M. E. *J. Chem. Phys.* **1988**, *89*, 2504.
(10) Fixman, M. *J. Chem. Phys.* **1965**, *42*, 3831. Pyun, C. W.; Fixman, M. *J. Chem. Phys.* **1965**, *42*, 3838. Fixman, M. *J. Chem. Phys.* **1966**, *44*, 2107. Fixman, M. *J. Chem. Phys.* **1966**, *45*, 793.
(11) Wiest, J. W.; Wedgewood, L. E.; Bird, R. B. *J. Chem. Phys.* **1989**, *90*, 587.
(12) Acierno, D.; Titomanlio, G.; Marrucci, G. *J. Polym. Sci., Polym. Phys. Ed.* **1974**, *12*, 2177.
(13) Rallison, J. M.; Hinch, E. J. *J. Non-Newtonian Fluid Mech.* **1988**, *29*, 37.
(14) Hinch, E. J. *J. Non-Newtonian Fluid Mech.* **1994**, *54*, 209.
(15) Larson, R. G. *Rheol. Acta* **1990**, *29*, 371.
(16) Liu, T. W. *J. Chem. Phys.* **1989**, *90*, 5826.
(17) Doyle, P.; Shaqfen, E. S. G.; Gast, A. P. *J. Fluid Mech* **1997**, *334*, 251.
(18) Larson, R. G.; Hu , H.; Smith, D. E.; Chu, S. *J. Rheol.* **1999**, *43*, 267.
(19) de Gennes, P. G. *Science* **1999**, *276*, 5321.
(20) Neuman, R. M. *J. Chem. Phys.* **1999**, *110*, 7513.
(21) Darinskii, A. A.; Saphiannikova, M. G. *J. Non-Cryst. Solid* **1994**, *172*−*174*, 932.
(22) Darinskii, A. A.; Saphiannikova, M. G.; Emri, I. *Polym. Sci. (Russ.)* **1995**, *37*, 1502.
(23) López Cascales, J. J.; García de la Torre, J. *J. Chem. Phys* **1991**, *95*, 9384. López Cascales, J. J.; García de la Torre, J. *J. Chem. Phys* **1992**, *97*, 4549. López Cascales, J. J.; García de la Torre, J. *J. Non-Cryst. Solid* **1994**, *172*, 823. López Cascales, J. J.; Díaz, F. G.; García de la Torre, J. *Polymer* **1995**, *36*, 345. Knudsen, K. D.; Hernandes Cifre, J. G.; García de la Torre, J. *Macromolecules* **1996**, *29*, 3603. Hernandes Cifre, J. G.; García de la Torre, J. *J. Non-Cryst. Solid* **1998**, *235*−*237*, 717. Hernandes Cifre J. G.; García de la Torre, J. *J. Rheol.* **1999**, *43*, 339.
(24) Fetsko, S. W.; Cummings, P. T. *J. Rheol.* **1995**, *39*, 285.
(25) Agarwal, U. S.; Bhargava, R.; Mashelkar, R. A. *J. Chem. Phys* **1998**, *108*, 1610. Agarwal, U. S. *J. Chem. Phys* **2000**, *113*, 3397.
(26) Neelov, I.; Lyulin, A.; Davies, G. R.; Adolf, D. B. *J. Chem. Phys.* **2002**, *33*, 3294.
(27) Ermak, D. L.; McCammon, J. A. *J. Chem. Phys.* **1978**, *69*, 1352.
(28) Öttinger, H. C. *Phys. Rev. E* **1994**, *50*, 2696. Öttinger, H. C. *Stochastic Processes in Polymeric Fluids*; Springer-Verlag: Heidelberg, Germany, 1996; p 244.
(29) Buhleiler, E.; Wehner, W.; Vögtle, F. *Synthesis* **1978**, 155.
(30) Tomalia, D. A.; Baker, H.; Dewald, J.; Hall, M.; Kallos, G.; Martin, S.; Roeck, J.; Ryder, J.; Smith, P. *Polym. J.* **1985**, *17*, 117.
(31) Johansson, M.; Malmström, E.; Hult, A. *J. Polym. Sci., Part A: Polym. Chem.* **1993**, *31*, 619.
(32) Fréchet, J. M. J.; Hawker, C. J.; Wooley, K. L. *J. M. S. −Pure Appl. Chem.* **1994**, *A31*, 1627.
(33) Peerlings, H. W. I.; Meijer, E. W. *Chem.—Eur. J.* **1997**, *3*, 1563.
(34) Zeng, F.; Zimmerman, S. C. *Chem. Rev.* **1997**, *97*, 1681.
(35) de Gennes, P. J.; Hervet, H. *J. Phys. Lett. Fr.* **1983**, *44*, L351.
(36) Naylor, A. M.; Goddard, W. A., III.; Kiefer, G. E.; Tomalia, D. A. *J. Am. Chem. Soc.* **1989**, *111*, 2339.

(37) Lescanec, R. L.; Muthukumar, M. *Macromolecules* **1990**, *23*, 2280.
(38) Mansfield, M. L.; Klushin, L. I. *Macromolecules* **1993**, *26*, 4262.
(39) Lue, L.; Prausnitz, J. M. *Macromolecules* **1997**, *30*, 6650.
(40) Chen, Z. Y.; Cui, S.-M. *Macromolecules* **1996**, *29*, 7943.
(41) Boris, D.; Rubinstein, M. *Macromolecules* **1996**, *29*, 7251.
(42) Sheng, Y.-J.; Jiang, S.; Tsao, H.-K. *Macromolecules* **2002**, *35*, 7865.
(43) Murat, M.; Grest, G. *Macromolecules* **1996**, *29*, 1278.
(44) Mazo, M. A.; Sheiko, S. S.; Zhilin, P. A.; Gusarova, E. B.; Balabaev, N. K. *Izvestia Akad. Nauk, Ser. Phys. (Russ.)* **1998**, *62*, 1098.
(45) Mansfield, M. L.; Klushin, L. I. *J. Phys. Chem.* **1992**, *96*, 3994. Mansfield, M. L. *Macromolecules* **2000**, *33*, 8043.
(46) Fixman, M. *J. Chem. Phys.* **1983**, *78*, 1588.
(47) Aerts, J. *Comput. Theor. Polym. Sci.* **1998**, *2*, 49.
(48) Widmann, A. H.; Davies, G. R. *Comput. Theor. Polym. Sci.* **1998**, *8*, 191.
(49) Cai, C.; Chen, Z. Y. *Macromolecules* **1998**, *31*, 6393.
(50) La Ferla, R. *J. Chem. Phys.* **1997**, *106*, 688.
(51) Lyulin, A.; Davies, G. R.; Adolf, D. B. *Macromolecules* **2000**, *33*, 3294. Lyulin, A.; Adolf, D. B.; Davies, G. R. *Macromolecules* **2000**, *33*, 6899.
(52) Lyulin, A.; Adolf, D. B.; Davies, G. R. *Macromolecules* **2001**, *34*, 3783.
(53) Sheridan, P. F.; Adolf, D. B.; Lyulin, A.; Neelov, I. M.; Davies, G. R. *J. Chem. Phys.* **2002**, *117*, 7802.
(54) Lee, A. T.; McHugh, A. J. *Macromol. Theory Simul.* **2001**, *10*, 244. Lee, A. T.; McHugh, A. J. *Macromol. Theory Simul* **2001**, *10*, 430.
(55) Rey, A.; Freire, J. J.; García de la Torre, J. *Macromolecules* **1987**, *20*, 2385.
(56) Rotne, J.; Prager, S. *J. Chem. Phys.* **1969**, *50*, 4831.
(57) Biswas, P.; Cherayil, B. J. *J. Chem. Phys* **1994**, *100*, 3201.
(58) Bird, R. B.; Curtiss, C. F.; Armstrong, R. C.; Hassager, O. Kinetic Theory. *Dynamics of Polymeric Liquids*, 2nd ed.; Wiley-Interscience: New York, 1987; Vol. 2.
(59) Larson, R. G.; Hu, H.; Smith, D. E.; Chu, S. *J. Rheol.* **1999**, *43*, 267.

MA030088B